Hindawi
Journal of Advanced Transportation
Volume 2022, Article ID 5879568, 13 pages
https://doi.org/10.1155/2022/5879568

Research Article

Differentiated Speed Planning for Connected and Automated Electric Vehicles at Signalized Intersections considering Dynamic Wireless Power Transfer

Lan Yang,[1] Mengjie Han,[1] Shan Fang,[1] Guoyuan Wu,[2] He Sheng,[1] Heng Wei,[3] and Xiangmo Zhao[1]

[1]*School of Information Engineering, Chang'an University, Xi'an, Shaanxi, China*
[2]*Center for Environmental Research and Technology, University of California at Riverside, Riverside, CA, USA*
[3]*ART-Engines Transportation Research Laboratory, College of Engineering and Applied Science, University of Cincinnati, OH, USA*

Correspondence should be addressed to Mengjie Han; han114336@163.com

Received 13 April 2022; Revised 25 July 2022; Accepted 15 September 2022; Published 10 October 2022

Academic Editor: Zhihong Yao

Deploying the dynamic wireless power transfer (DWPT) equipment at intersections can improve the transportation efficiency and decrease the energy consumption. It can easily turn the disadvantages of waiting time for red phase into the advantages of charging benefits for electric vehicles (EVs). This study develops a multiobjective speed planning model with differentiated charging strategy to optimize the EV's trajectory at signalized intersections with DWPT. To mitigate the negative impact of DWPT, the proposed model is divided into charging priority driving (C-eco-driving) mode and time priority driving (T-eco-driving) mode for connected and automated electric vehicles (CAEVs) to apply different scenarios. Meanwhile, a widely applied car-following model, i.e., the Intelligent Driver Model (IDM), has been calibrated with the ground-truth dataset to meet the intersection characteristic for EVs in mixed traffic. The efficiency and robustness of two eco-driving modes were validated in single-vehicle and mixed traffic based on MATLAB simulation. For single vehicle, the electricity benefits of the C-eco-driving mode and T-eco-driving mode increase about 0.0867 kWh and 0.0532 kWh, respectively. T-eco-driving mode reduces 2.5 s of travel time. For mixed traffic, the C-eco-driving mode provides more charging benefits about 51~73% than no-control strategy. In contrast, the T-eco-driving mode provides significant time benefits of 2.6 s and slight electricity benefits of 12~30% than no-control strategy. The increment of market penetration rate and wireless charging length can significantly improve the charging benefits. When charging length has the same value, the closer the DWPT facilities to the intersection, the more obvious the charging benefits.

1. Introduction

EVs have been recognized as an effective means of achieving energy conservation and sustainable development in recent years [1–4]. Governments have implemented various policies and regulations to encourage the popularization of EVs, including a green-car subsidy program and license plate bias [5]. With this momentum, EVs will phase out fuel vehicles in the near future.

Due to the limited battery capacity and short driving range, EVs require frequent charging. The widespread adoption of EVs may result in an increase in charging demand. As a result, many charging stations, battery swap stations, and wireless charging equipment have been constructed to meet the demands for charging [6–8]. The construction of charging station has low cost, but charging waiting time for EVs is long, and the fast-charging technology can decrease the battery life [9]. The advantage of the battery

swap station is the short charging time; the disadvantage is the unstandardized battery [10]. For wireless charging, EVs can achieve electricity supplements when traveling at the wireless charging lanes. It is more convenient and safer than other charging infrastructures [11–13].

A few studies have concentrated on the competitive analysis of different types of charging infrastructures [14–16]. Based on the charging demands of electric public transit system, Chen et al. [17] established mathematical models to achieve the optimal deployment of various charging facilities, and the DWPT technology is more competitive than charging stations and battery swapping stations with low service frequency and high operating speed. To address the range and recharge issues for EVs, Fuller [18] concluded that dynamic wireless charging can be a more cost-effective approach to extending driving range than increasing battery capacity. Thus, it can be seen that DWPT will play a significant role in future charging technology field.

When deploying the DWPT along ingress lanes at intersections or arterial, it can easily achieve electricity benefits for EVs [19–21]. Therefore, some researches focused on the influence of wireless charging lanes on traffic system. He et al. [22, 23] investigated the impacts of the dynamic charging lane on EV's motion behavior, and the results show that the each EV could run slowly on the charging lane with causing low traffic efficiency. To improve the traffic efficiency, He et al. [24] established a model to optimize the location of the charging lane by considering their adverse effects on road capacity. To address the optimal deployment problem at signalized arterial, Li et al. [25] proposed a biobjective model considering both traffic efficiency and charging facilities' utilization rate. The results show that DWPT equipment is more suitable to be installed near intersections. Based on this theory, Mohrehkesh and Nadeem [26] proposed a wireless charging scheme for the battery electric vehicles and investigated how to integrate control strategies at intersections but have not established a specific speed guidance model for EVs. Subsequently, Zhang et al. [27] proposed an eco-driving control strategy for CAEVs at signalized intersections with charging lane.

To sum up, the DWPT technology can decrease partially traffic operation efficiency but can increase the charging efficiency. To mitigate the negative impacts of DWPT technology, this paper proposed a new scheme for CAEVs at intersections. Two driving control strategies are investigated to apply different scenarios. The charging priority control strategy is more suitable for the following scenarios: (1) long red phase waiting time, (2) low traffic flow, and (3) low state of charge (SOC) for EVs. The time priority control strategy is more suitable for the following scenarios: (1) high traffic flow and (2) high SOC for EVs. The scheme of differentiated strategy can easily reduce disadvantage of DWPT in traffic efficiency, meanwhile significantly improving the advantage of DWPT in electricity benefits. As a result, the speed planning strategy for CAEVs should consider a variety of optimization factors, such as traffic efficiency, electricity consumption, and driver comfort.

In this study, a multiobjective speed planning model based on differentiated control strategy at a signalized intersection with DWPT is proposed. Based on the SOC of EVs entering the control segment, the model is divided into C-eco-driving and T-eco-driving by adjusting three weight coefficients. The Next-Generation Simulation (NGSIM) dataset is used to calibrate the car-following model for the EV in mixed traffic. Numerical studies of single-vehicle and mixed traffic are used to validate the efficiency and adaptability of the speed planning model.

The remainder of this paper is composed as follows. Section 2 provides the scenario description for EVs traversing intersections with DWPT. Section 3 describes the differentiated speed planning model and the calibrated IDM. Next, the single-vehicle and mixed-traffic examples are carried out to demonstrate the efficiency and adaptability of the proposed model in Section 4. Finally, the concluding remark is presented in Section 5.

2. Scenario Description

As shown in Figure 1, a signalized intersection with DWPT is established, and vehicle queues consisting of CAEVs and human-driven EVs pass through the intersection. The total control segment's start position is O, and its length is S. $\mathrm{WCL}(S_1, S_2)$ denotes that the start position of deploying the wireless charging transfer is S_1, and the terminal location is S_2. The length of wireless charging is $(S_2 - S_1)$. The position of the intersection stop line is S_3. When the CAEV enters the control segment of a signalized intersection, it is assumed that it can obtain certain information via V2I and V2V communications, such as the distance to the stop bar, SPaT information, the location and length of the charging area, and the states of preceding vehicles, which are not available to regular EVs. When mixed vehicles enter the control segment, the CAEV will follow the proposed model's trajectory planning advice to navigate the intersection smoothly and avoid stopping. In contrast, the regular EV will follow the designated car-following model. Two distinct planning strategies for CAEV are considered in this study in order to meet varying demands. As illustrated in Figure 1, low-battery CAEVs may prefer the charging priority driving strategy, whereas high-battery CAEVs may prefer the time priority driving strategy. The former is concerned with electricity, whereas the latter is concerned with time and driving comfort.

3. Two Models at a Signalized Intersection with DWPT

3.1. Differentiated Speed Planning Model for the CAEV

3.1.1. Multiobjective Optimization. To guide CAEVs passing through signalized intersections safely and efficiently, the model optimization objective sets three factors: traffic efficiency, electricity consumption, and driver comfort. Since three factors have different units and dimensions and orders of magnitude, when three factors are directly added together, the role of the factor with a larger value in the objective function will be highlighted. Therefore, this paper standardizes them to eliminate the influence of different dimensions.

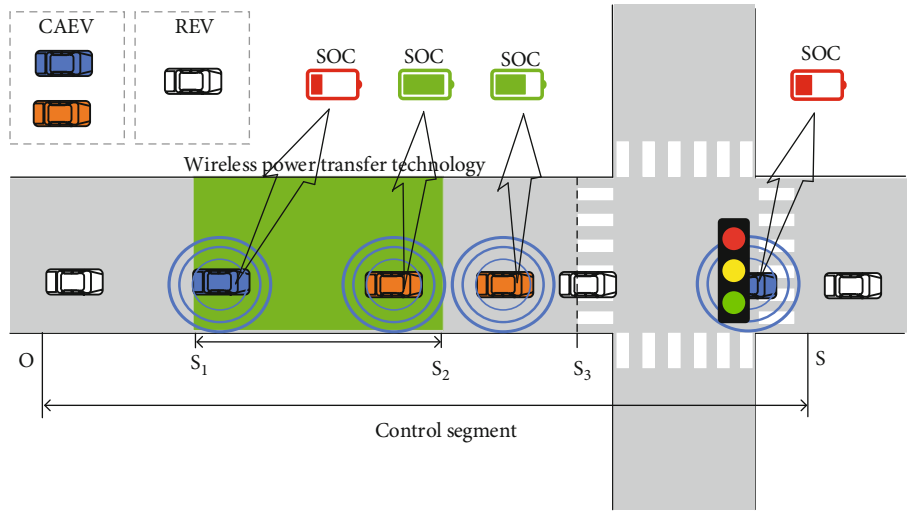

Figure 1: The scenario with differentiated driving strategy at the signalized intersection with the DWPT.

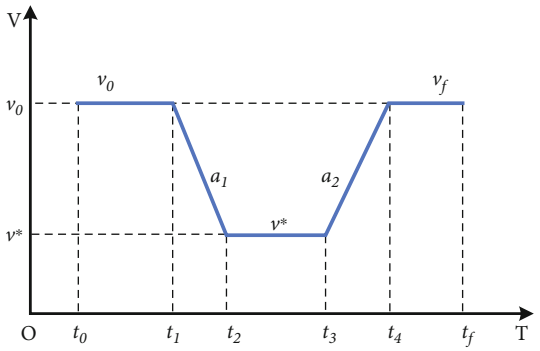

Figure 2: Entire process of speed planning.

Table 1: Weighting parameters of two driving modes.

Parameters	C-eco-driving	T-eco-driving
ω_1	0.1~0.2	0.4~0.6
ω_2	0.6~0.8	0.1~0.2
ω_3	0.1~0.2	0.2~0.4

(1) Traffic efficiency optimization

This study improves the efficiency of traffic flow by reducing the guidance time of vehicles in the control segment, while avoiding the behavior of stop-go at signalized intersections. Therefore, the efficiency optimization formula is

$$F_t = \left(t_f - t_0 - T_{\min}\right)/\left(T_{\max} - T_{\min}\right), \tag{1}$$

$$T_{\max} = \max_{i=1\cdots n}\left\{t_f(i) - t_0(i)\right\}, \tag{2}$$

$$T_{\min} = \min_{i=1\cdots n}\left\{t_f(i) - t_0(i)\right\}, \tag{3}$$

where F_t is the efficiency objective value; t_0 and t_f are the initial time and terminal time of the control segment; $T_{\min}$ and $T_{\max}$ are the shortest and longest travel times in all historical trajectories, respectively; and n is the number of historical trajectories.

(2) Electricity consumption optimization

The vehicle's SOC is not only influenced by the electricity loss of the traction but also supplemented by DWPT facility and the regenerative braking system (RBS). It can be formulated as follows:

$$\begin{aligned} F_e &= \frac{\left(E_{\mathrm{NC}} - E_{\mathrm{Charge}} - E_{\min}\right)}{\left(E_{\max} - E_{\min}\right)}, \\ E_{\mathrm{NC}} &= E_{\mathrm{Consumption}} - E_{\mathrm{Recovery}}, \\ E_{\mathrm{Charge}} &= P_{\mathrm{Charge}} T_{\mathrm{Charge}}, \\ E_{\max} &= \max_{i=1\cdots n}\left\{E_{\mathrm{NC}}(i) - E_{\mathrm{Charge}}(i)\right\}, \\ E_{\mathrm{mix}} &= \min_{i=1\cdots n}\left\{E_{\mathrm{NC}}(i) - E_{\mathrm{Charge}}(i)\right\}, \end{aligned} \tag{4}$$

where F_e is the electricity objective value; E_{NC} is the electricity consumption that has considered RBS; and E_{Charge} is the charging electricity with DWPT. $E_{\min}$ and $E_{\max}$ are the minimum and maximum total electricity consumption in all historical trajectories, respectively.

(3) Driver comfort optimization

This study optimizes the driver comfort by reducing the speed fluctuation of CAEVs during the control segment. The formula is shown as follows:

$$F_s = \frac{\left(\int_{t_0}^{t_f} a^2(t)dt - U_{\min}\right)}{\left(U_{\max} - U_{\min}\right)}, \tag{5}$$

1 Step 1. Data preprocessing
2 Remove exception data and out-of-bound data from the original data.
3 Select continuous four state vectors for FVs: speed, space difference, speed difference, and acceleration.
4 Unit conversion, such as ft, ft/s to m, and m/s.
5 Step 2. Initialization
6 Randomly generate the initial values for five calibrated parameters within the bound, a, b, s_0, T, and v_0.
7 Initialize GA basic parameters, such as maximum iteration, population size, and crossfactor.
8 Step 3. Fitness function
9 Estimate the acceleration (predictive value) for FV at the next time point using Equations (17) and (18).
10 Evaluate RMSE between predictive value and true value with Equation (19).
11 Step 4. Update five calibrated parameters
12 Update five parameters with fitness function.
13 Step 5. Termination condition
14 If the number of iteration is larger than the maximum value or RMSE is not larger than the specified gap, stop the algorithm. Otherwise, go back to Step 3.

Algorithm 1: IDM parameter calibration algorithm based on GA.

Table 2: IDM parameter calibration results.

Parameters	Description	Bounds	Calibrated
a (m/s^2)	Acceleration	[0.1, 5]	4.1
b (m/s^2)	Deceleration	[0.1, 5]	3.7
s_0 (m)	Minimum distance	[0.1, 10]	5.68
T (s)	Time gap	[0.1, 5]	1.5
v_0 (km/h)	Desired speed	[1, 150]	72.3

Table 3: Parameters used in simulations.

Parameters	Values	Parameters	Values
$v_{\max}$ (m/s)	22	η_d	0.92
$v_{\min}$ (m/s)	2.00	η_m	0.91
$a_{\max}$ (m/s^2)	4.88	η_b	0.90
$a_{\min}$ (m/s^2)	-3.41	α	0.0411
m (kg)	1521	P_{Charge} (kW)	20
θ	0	W (kWh)	60
C_r	1.75	S_3 (m)	500
c_1	0.0328	S (m)	550
c_2	4.575	T_{red} (s)	35
A_f (m^2)	2.3316	T_{green} (s)	45
C_D	0.28	t_{entry} (s)	0
Threshold	0.5		

$$U_{\max} = \max_{i=1\cdots n}\left\{\int_{t_0(i)}^{t_f(i)} a^2(t)dt\right\}, \tag{6}$$

$$U_{\min} = \min_{i=1\cdots n}\left\{\int_{t_0(i)}^{t_f(i)} a^2(t)dt\right\}, \tag{7}$$

where F_s is the stability objective value and $U_{\min}$ and $U_{\max}$ are the minimum and maximum speed fluctuations in all historical trajectories, respectively.

(4) Three-objective optimization function

Based on the above, we integrate three optimizations by applying three weighting coefficients:

$$\begin{aligned} \min_{a(t)} L &= \omega_1 F_t + \omega_2 F_e + \omega_3 F_s, \\ \omega_1 + \omega_2 + \omega_3 &= 1, \\ 0 < \omega_i &< 1, \quad i = 1, 2, 3, \end{aligned} \tag{8}$$

where L is the objective value and ω_1, ω_2, and ω_3 are weights for different objectives, presenting the importance of time, electricity, and stability, respectively. Three weighting coefficients can be dynamically adjusted to achieve differentiated travel demands.

3.1.2. Dynamic Constraints. The objective function for CAEV is subject to the following constraints:

(1) Motion state definitions and initial state declarations are formulated as follows:

$$\begin{aligned} \dot{x}(t) \triangleq [v(t), a(t)]^T &= f(x(t), u(t)), \quad t_0 \le t \le t_f, \\ s(t_0) = 0, v(t_0) &= v_0, \end{aligned} \tag{9}$$

where $x(t)$ is the state vector of the EV at time t and $s(t)$, $v(t)$, and $a(t)$ are distance, speed, and acceleration at time t, respectively. Because the detector is set at the starting point of the control segment, the initial coordinate for CAEVs is 0.

(2) The vehicle distance constraint is defined as the distance characteristic that the vehicle satisfies within the control segment:

$$s(t_{s1}) = S_1 \quad s(t_{s2}) = S_2, \tag{10}$$

$$s(t_{s3}) = S_3 \quad s(t_f) = S, \tag{11}$$

Table 4: Parameter setting of eight scenarios.

Scenario	Initial speed (m/s)	WCL (m)	Scenario	Initial speed (m/s)	WCL (m)
A	16	(50, 250)	E	20	(50, 150)
B	18	(50, 250)	F	20	(50, 250)
C	20	(50, 250)	G	20	(50, 350)
D	22	(50, 250)	H	20	(50, 450)

$$s_k(t) < s_{k-1}(t), \tag{12}$$

where t_{s1} and t_{s2} are the entry time and exit time in the wireless charging area, respectively, and t_{s3} is the arrival time at the stop line S_3. Equation (12) is the safe distance constraint.

(3) Vehicle kinematic constraints declare the physical boundaries of vehicle speed and acceleration:

$$\begin{aligned} v_{\min} \le v(t) \le v_{\max}, \\ a_{\min} \le a(t) \le a_{\max}, \end{aligned} \tag{13}$$

where $v_{\min}$ and $v_{\max}$ are the maximum speed, respectively, and $a_{\min}$ and $a_{\max}$ are minimum and maximum accelerations. The maximum speed is the legal limit on the road, and the minimum speed is a reasonable threshold to avoid the vehicle traveling at very low speeds in the charging area.

(4) Traffic state constraint that ensures the EV can pass through the signalized intersection during the green time:

$$\begin{aligned} t_{\min} \le t_{s3} \le t_{\max}, \\ t_{\min} = T_r + kT, t_{\max} = T_r + G + kT \text{ if signal}_{t_0} = \text{red}, \\ t_{\min} = 0, t_{\max} = T_g \text{ if signal}_{t_0} = \text{green}, \\ t_{\min} = T_g + R + kT, t_{\max} = T_g + (k+1)T \text{ if signal}_{t_0} = \text{green}, \end{aligned} \tag{14}$$

where $k = 0, 1, 2 \cdots$, $t_{\min}$ and $t_{\max}$ are the shortest time and the longest time, respectively; T_r and T_g are the red light or green light duration when the vehicle enters the segment; R and G are the red and green periods, respectively; T is the traffic phase period; and signal_{t_0} is the phase state at the initial time.

3.1.3. Model Regularization. To achieve high computational efficiency for real-time control, this study numerically discretizes time and space dimensions into a series of collocation points using metaheuristics or gradient-based methods and regularizes the speed profile of the entire process by consulting reference [27, 28]. The entire speed planning process can be divided into five phases, as illustrated in Figure 2.

(1) Cruise at the initial speed v_0 from t_0 to t_1

(2) Decelerate at a constant rate a_1 from t_1 to t_2

(3) Cruise at a specific speed v^* from t_2 to t_3

(4) Accelerate at a constant rate a_2 from t_3 to t_4

(5) Cruise at the terminal speed v_f from t_4 to t_f

The initial speed v_0 is assumed to be the same value with v_f in the control segment, which contents the characteristics of the wireless charging scheme.

$$\begin{aligned} t_0 \le t_1 \le t_2 \le t_3 \le t_4 \le t_f, \\ v_0 = v_f, \\ a_1 = \frac{2(S_3 - v_0(t_{s3} - t_0))}{(t_2 - t_1)(t_4 + t_3 - t_2 - t_1)}, \\ a_2 = -\frac{t_2 - t_1}{t_4 - t_3} a_1, \\ v^* = v_0 + (t_2 - t_1)a_1, \end{aligned} \tag{15}$$

where v^* is the minimum speed of the control segment. a_1 and a_2 are deceleration and acceleration, respectively. Therefore, Equation (8) can be simplified, as shown in Equation (16).

$$\begin{cases} \min\limits_{t_1, t_2, t_3, t_4} L = \omega_1 \left(\dfrac{t_f - t_0 - T_{\min}}{T_{\max} - T_{\min}} \right) + \omega_2 \left(\dfrac{E_{\text{NC}} - E_{\text{Charge}} - E_{\min}}{E_{\max} - E_{\min}} \right) + \omega_3 \left(\dfrac{\int_{t_0}^{t_f} a^2(t)dt - U_{\min}}{U_{\max} - U_{\min}} \right) \\ \text{s.t.Equations (9) – (15)} \end{cases} \tag{16}$$

The proposed model is solved by the Particle Swarm Optimization (PSO) algorithm [29]. The comprehensive power-based energy consumption model is used to estimate the energy consumption [30].

3.1.4. Differentiated Travel Mode. The value of weighting coefficient represents different driving strategies. By adjusting the values of ω_1, ω_2, and ω_3, the proposed model is divided into C-eco-driving mode and T-eco-driving mode. Table 1 shows the value range of two modes. The coefficient is set to a range of values rather than fixed values to ensure dynamicity.

For C-eco-driving mode, when the SOC of CAEV entering to the segment is below the threshold, the strategy focuses on the charging efficiency. Thus, ω_2 is set as primary weighting coefficient (0.6~0.8), as the upper bound of C-eco-driving mode; ω_1 and ω_3 are set as secondary weighting coefficient (0.1~0.2), as the lower bound of C-eco-driving mode. Only considering electricity ($\omega_1\omega_2, \omega_3 = 0, 1, 0$) is likely to cause the vehicle to remain stationary in the charging area, which makes the model unsolvable.

For the T-eco-driving mode, when the SOC of CAEV entering to the segment is above the threshold, the strategy focuses on the traffic efficiency. ω_1 is set as the first

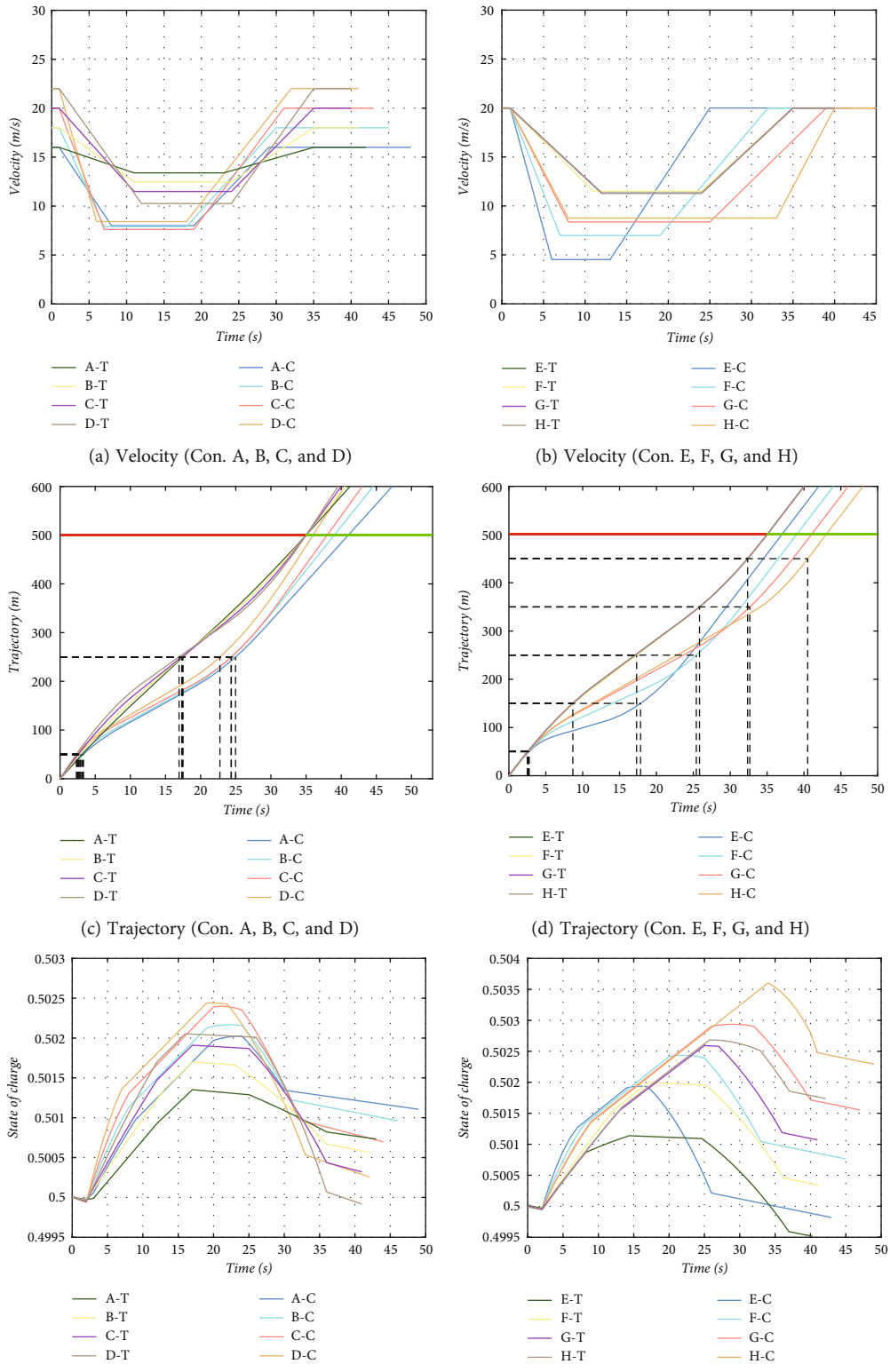

(a) Velocity (Con. A, B, C, and D)

(b) Velocity (Con. E, F, G, and H)

(c) Trajectory (Con. A, B, C, and D)

(d) Trajectory (Con. E, F, G, and H)

(e) State of charge (Con. A, B, C, and D)

(f) State of charge (Con. E, F, G, and H)

Figure 3: Results of eight scenarios.

weighting coefficient (0.4~0.6) to achieve high traffic efficiency. ω_3 is set as the second weighting coefficient (0.2~0.4) to avoid the occurrence of large speed fluctuations. ω_2 is set as the third weighting coefficient to ensure that speed fluctuation is adjusted in the direction of increasing electricity benefits.

Table 5: Numerical results under eight scenarios.

Con.	t_f (s)	E_{cha} (Ws)	E_{con} (Ws)	E_{rec} (Ws)	Con.	t_f (s)	E_{cha} (Ws)	E_{con} (Ws)	E_{rec} (Ws)
A-C	45.0	430612	274757	96390	A-T	39.0	286859	146650	26886
B-C	42.0	425701	360127	131887	B-T	38.0	291260	245521	75750
C-C	43.0	471664	473915	180412	C-T	38.0	295516	354387	128464
D-C	39.0	404445	543897	206228	D-T	38.0	291191	481342	184875
E-C	43.0	365223	535568	189656	E-T	38.0	123058	356885	129217
F-C	43.0	471664	473915	180412	F-T	38.0	295516	354387	128464
G-C	43.0	576075	416312	161602	G-T	38.0	465161	356885	129217
H-C	43.0	691393	378857	145336	H-T	38.0	595830	356885	129217

Table 6: Attribute settings in mixed traffic.

Attributes	Value
Initial speed of the EV	16~22 m/s
Initial speed of the CAEV	18~20 m/s
Initial headway	30~60 m
Penetration rate	0~100%
Wireless charging length	100~400 m

Table 7: Parameter settings of six numerical examples.

Condition	MPR (%)	WCL (m)	Condition	MPR (%)	WCL (m)
I	0	(50, 250)	IV	60	(50, 250)
II	20	(50, 250)	V	80	(50, 250)
III	40	(50, 250)	VI	100	(50, 250)

ω_3 is not set as the first weighting coefficient as the comfort priority mode. The reason is that only considering driver comfort without considering travel time and SOC does not satisfy the real demands.

3.2. Calibrated Car-Following Model for the EV. The IDM [31] is an accident-free model capable of producing realistic acceleration profiles, and it can accurately simulate various traffic flow scenarios. Therefore, this study applies IDM to plan the trajectory for EVs. As defined in Equation (17) and Equation (18):

$$\dot{v} = a\left[1 - \left(\frac{v}{v_0}\right)^{\delta} - \left(\frac{s^*(v,\Delta v)}{s}\right)^2\right], \tag{17}$$

$$s^*(v,\Delta v) = s_0 + \max\left(0, vT + \frac{v\Delta v}{2\sqrt{ab}}\right), \tag{18}$$

where v, a, and b are the speed, acceleration, and deceleration of the following vehicle, respectively; s, s_0, and s^* are the current distance, minimum distance, and desired distance, respectively; v_0 is the desired speed; δ is the acceleration; Δv is the speed difference between the preceding vehicle and following vehicle; and T is the time gap that means following vehicle's reaction time.

Model calibration refers to parameter calibration, and different parameters typically reflect different driving characteristics. To meet the intersection characteristic, the NGSIM dataset [32], collected from a segment of Lankershim-Boulevard in Los Angeles, California, is used to calibrate the IDM. A genetic algorithm [33] is used to calibrate the five major parameters of IDM, such as a, b, s_0, T, and v_0. The Root Mean Square Error (RMSE) was used evaluate the difference between predicted values and true values, whose formula is as follows:

$$\mathrm{RMSE} = \sqrt{\frac{1}{n}\sum_{i=1}^{n}(\hat{a}_i - a_i)^2}, \tag{19}$$

where $\hat{y} = \{\hat{a}_1, \hat{a}_2, \cdots, \hat{a}_n\}$ are predicted values; $y = \{a_1, a_2, \cdots, a_n\}$ are true values; and n denotes the number of all data points.

Based on the preceding discussion, Algorithm 1 presents the pseudocode for the calibration method. Table 2 shows the calibration results for the IDM. The bounds of calibrated parameters refer to the literature [34].

4. Numerical Studies

To validate the effectiveness and adaptability of the proposed model, single-vehicle and mixed traffic is performed under various numerical examples based on MTALB simulation. Table 3 shows the basic parameters of numerical simulations.

4.1. Single-Vehicle Simulation under Different Initial Speeds and Wireless Charging Lengths. The initial speed of vehicles and wireless charging length (WCL) are used as variables in single-vehicle simulation. This paper built eight scenarios to evaluate the traffic benefits of the proposed model. As shown in Table 4, scenarios A, B, C, and D are used to compare each other with different initial speeds when the WCL is fixed. Scenarios E, F, G, and H are used to compare each other with different WCLs when the initial speed is fixed.

Figure 3 depicts the velocity, trajectory, and SOC of CAEVs. According to Figure 3(a), the vehicle with the T-eco-driving mode has higher speed than that with the C-eco-driving mode in total, and the CAEV with the T-eco-driving mode has less speed fluctuation than that with the

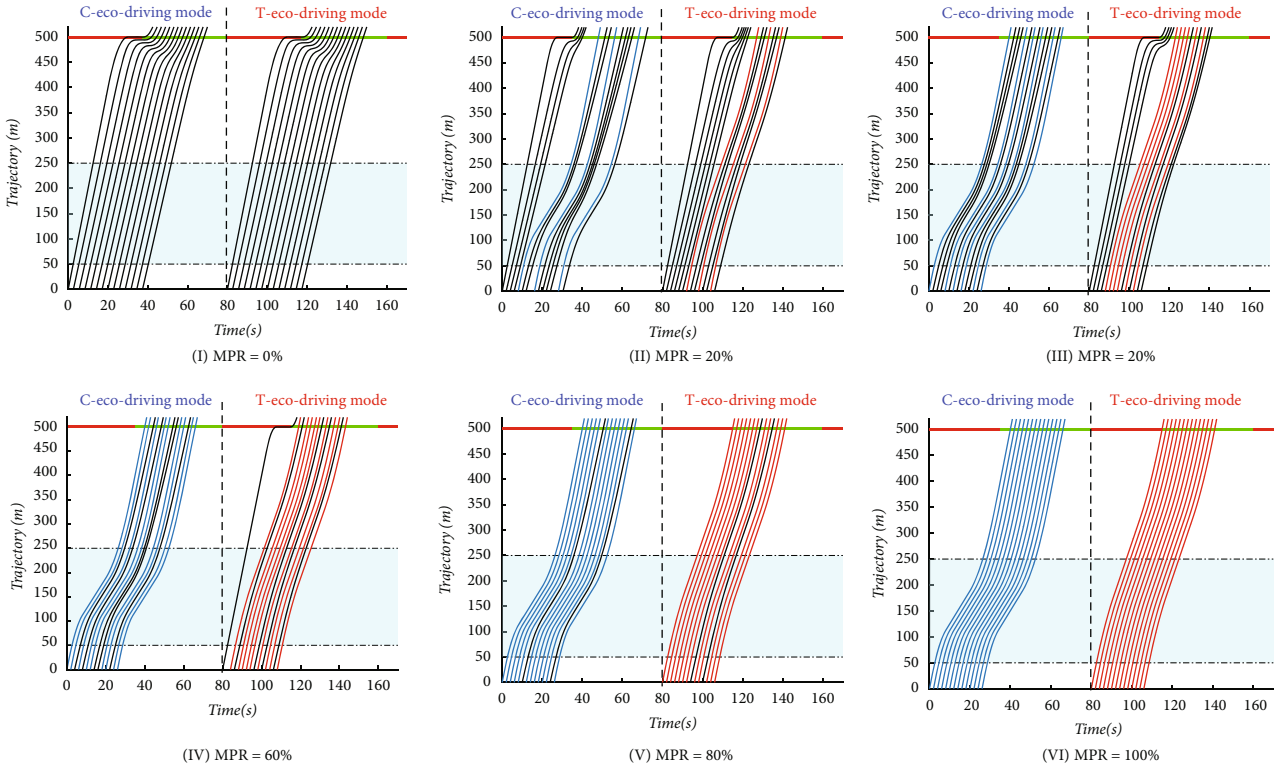

Figure 4: Spatial-temporal trajectories of six conditions (I~VI).

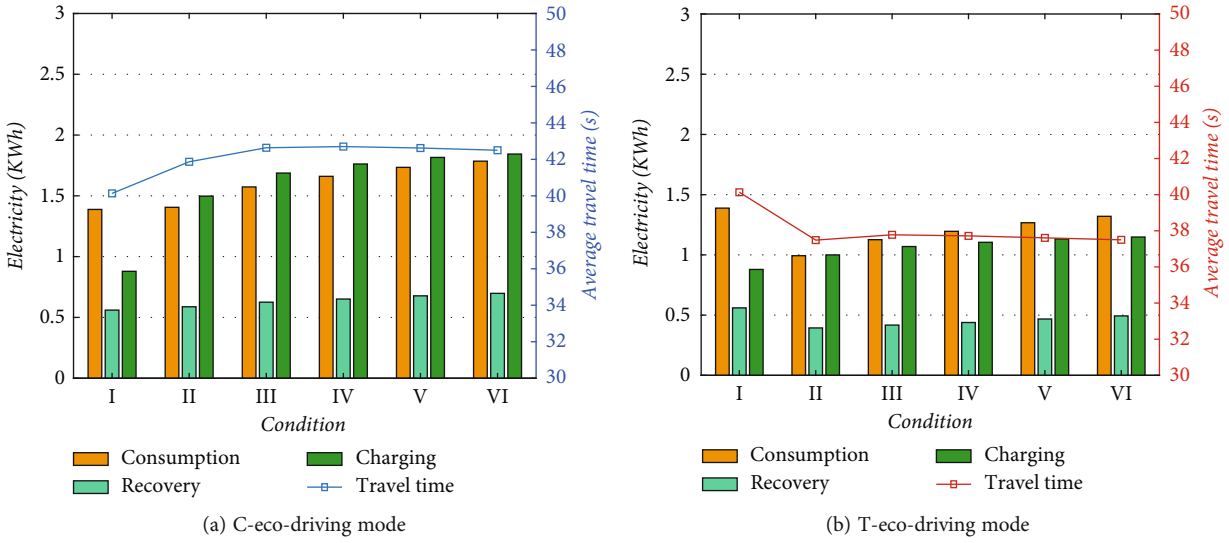

Figure 5: Electricity usage (consumption, recovery, and charging) and average travel time of six conditions (I~VI).

Table 8: Parameter settings of four numerical examples.

Condition	MPR (%)	WCL (m)	Condition	MPR (%)	WCL (m)
VII	40	(50, 150)	IX	40	(50, 350)
VIII	40	(50, 250)	X	50	(50, 450)

C-eco-driving mode. It demonstrates the significance of time and stability for the T-eco-driving mode. More specifically, for the T-eco-driving mode, the minimum speed v^* within the control segment declines when the initial speed continuously increases. However, the minimum speed v^* remains relatively stable as the initial speed increases for the C-eco-driving mode. The main reason is that the weighting coefficient ω_3 is different. From Figure 3(b), for the T-eco-driving mode, the speed of four scenarios basically overlaps. For the

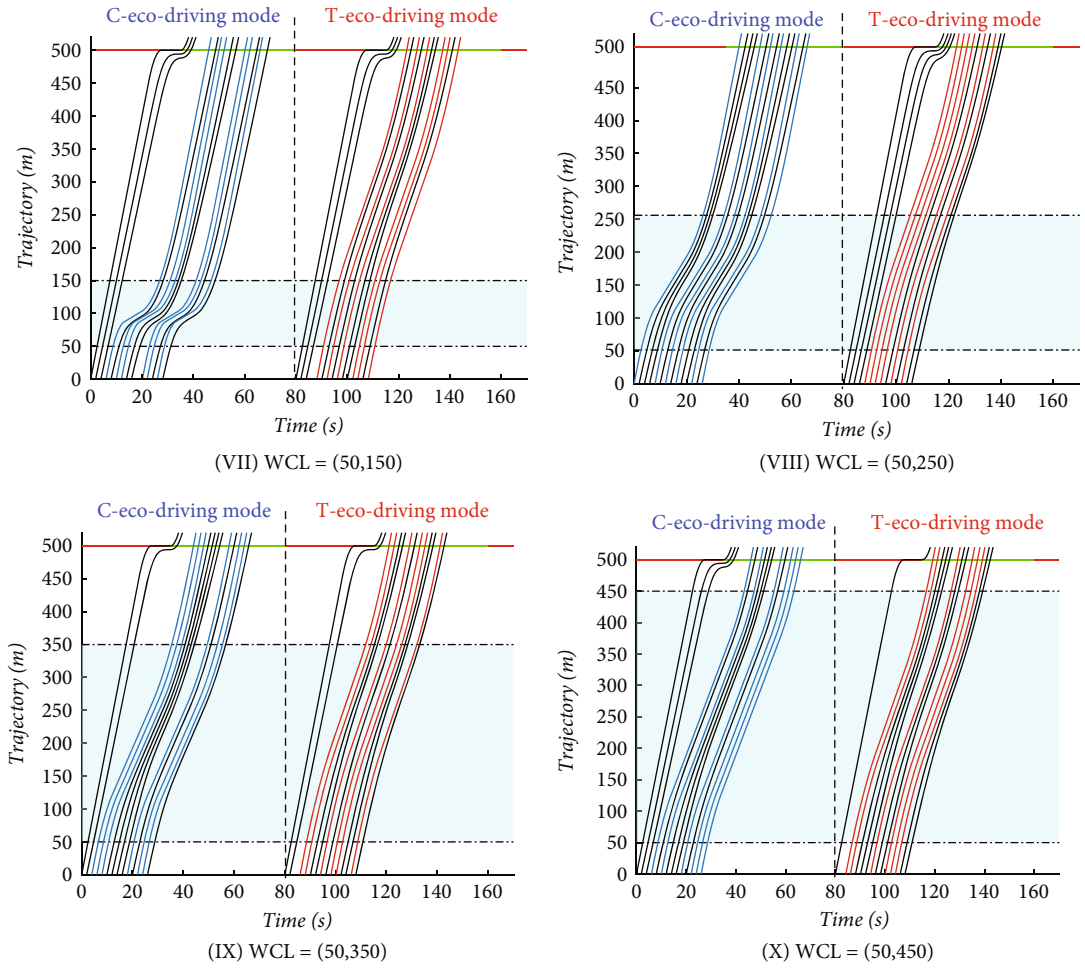

Figure 6: Spatial-temporal trajectories of four conditions (VII~X).

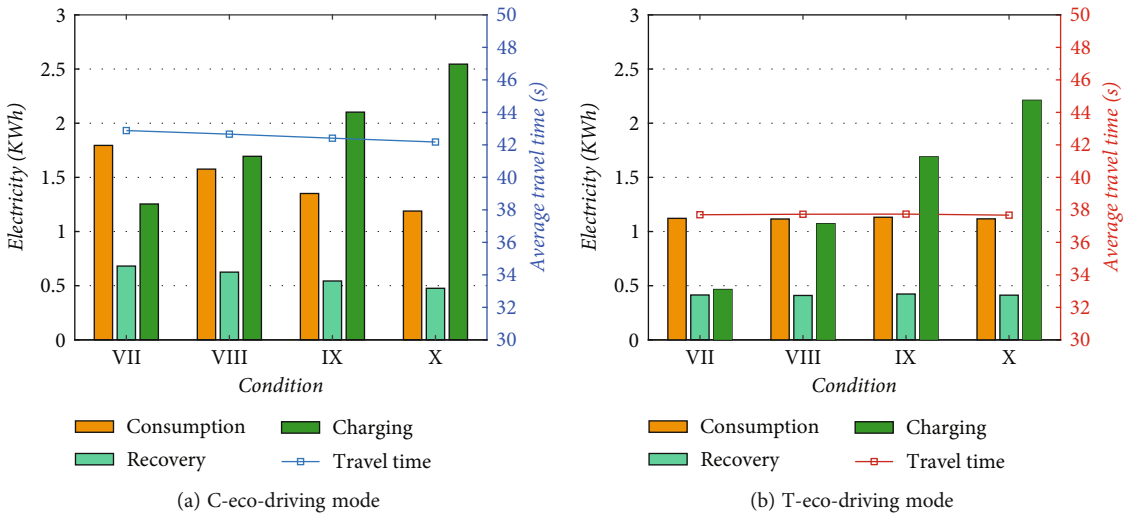

Figure 7: Electricity usage (consumption, recovery, and charging) and average travel time under four conditions (VII~X).

C-eco-driving mode, the value of v^* maintains an upward trend and cruise time at the speed v^* becomes longer with the extension of the wireless charging area (WCA). It is easily inferred that the upward is limited.

Figures 3(c) and 3 (d) depict the trajectory results of eight scenarios for the CAEV. The dotted lines indicate the point of entering and exiting the charging area. As shown in Figure 3(c), for the T-eco-driving mode, the vehicle

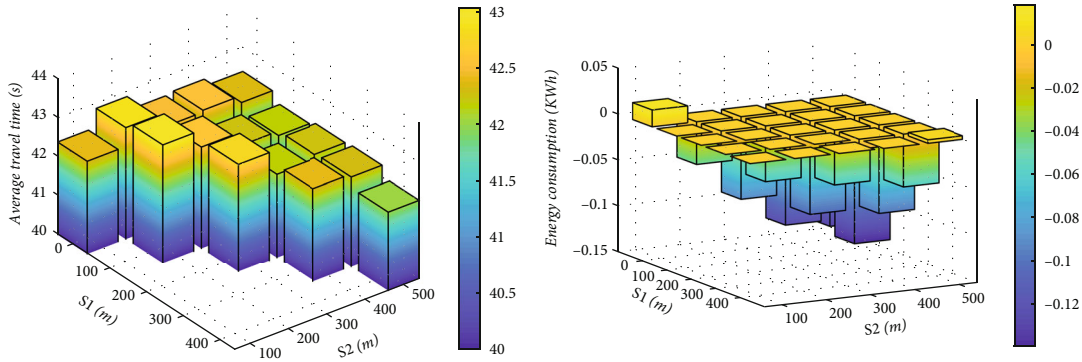

(a) Average travel time (b) Total electricity consumption

FIGURE 8: Traffic benefits of different charging locations in mixed traffic.

arrives at the intersection in 35 seconds, and the total time spent traversing the control segment is approximately 40 seconds. For the C-eco-driving mode, the arrival time at the intersection is 36 s, 39 s, 41 s, and 43 s, respectively. The total time is approximately 45 seconds. It implies that the vehicle with the T-eco-driving mode takes less time to pass through an intersection than the C-eco-driving mode. According to Figure 3(d), trajectories under four scenarios are consistent due to speed profile overlap for the T-eco-driving mode. The charging duration of the CAEV increases with the extension of the charging lane for the C-eco-driving mode. Similarly, the CAEV with the T-eco-driving mode takes less time than the C-eco-driving mode.

Furthermore, Figures 3(e) and 3 (f) depict the SOC of the CAEV. The battery's maximum capacity is assumed to be 60 kWh, and the initial SOC is 0.5. Overall, the CAEV with the C-eco-driving mode has more electricity than the T-eco-driving mode, indicating the importance of charging electricity for the C-eco-driving mode. Based on the RBS system, the SOC of the CAEV regularly rises when the vehicle operates rapidly deceleration or drives in a wireless charging area, and SOC falls when the vehicle accelerates rapidly. According to Figure 3(e), regardless of which eco-driving mode the CAEV uses, the terminal SOC rises with the increase of the initial speed. It implies that the initial speed has a significant impact on the model's performance. As illustrated in Figure 3(f), the longer the WCL, the greater the charging benefits. The DWPT technology has the potential to significantly promote electricity for two eco-driving modes. Numerical results show that the benefit in electricity replenishment for the C-eco-driving mode is 0.114~0.216 kWh, and the benefit for the T-eco-driving mode is 0.066~0.162 kWh.

Detailed numerical results under eight scenarios have been shown in Table 5. Four metrics are used for evaluation. t_f is the terminal time; E_{cha} is the recharge energy within the charging area; E_{con} is the energy consumption; E_{rec} is the recovered energy due to RBS.

4.2. Mixed-Traffic Simulation with Different Market Penetration Rates, Charging Lengths, and Locations. In mixed-traffic simulation, the market penetration rate (MPR) of CAEV, charging lengths, and locations are used as variables to analyze the adaptability of the proposed model. As shown in Table 6, the fluctuation of the initial status is considered to better evaluate the robustness of the model.

4.2.1. Adaptability Analysis of Different MPRs. To analyze the traffic benefits of different MPRs, six numerical examples are used to validate the model adaptability. As shown in Table 7, when charging area is set to (50, 250) as the constant value, the MPR is set to the variable value ranging from 0% to 100%.

Figure 4 depicts the spatial-temporal trajectories of approximately 28 vehicles under six conditions (I~VI). The trajectories of vehicles controlled by the C-eco-driving mode, T-eco-driving mode, and calibrated IDM are shown in blue, red, and black lines, respectively. In general, at a higher penetration rate, many regular EVs are more likely to drive on suboptimal trajectories due to car-following characteristics, and these EVs could take advantage of DWPT and travel on a suboptimal trajectory with a low delay. However, the benefit of a moderate penetration rate is highly fluctuant. For instance, in the left of Figure 4 (III), the lead vehicle is a CAEV which can advantageously guide rear vehicles. In contrast, the lead vehicle is a regular EV which cannot benefitly guide following vehicles in the right of Figure 4 (III). As a result, benefit performance is strongly related to the type of the lead vehicle.

Figure 5 shows the average travel time and electricity usage under six conditions for two eco-driving modes. As shown in Figure 5(a), for the C-eco-driving mode, as MPR increases, electricity consumption slowly rises from 1.39 kWh to 1.84 kWh, and electricity recovery remains stable at 0.56~0.69 kWh. Compared to scenario I, electricity charging in scenarios II~VI increases dramatically, with a growth rate ranging from 70.4% to 100.1%. It demonstrates the advantage of the C-eco-driving mode when recharging electricity. Under scenarios II~VI, the average travel time increases slightly; it is unavoidable to sacrifice a little travel time due to the slow speed of vehicles in exchange for more charge. For the T-eco-driving mode from Figure 5(b), compared to scenario I, the electricity consumption and recovery under scenarios II~VI decrease certainly, by approximately 4.9~28.2% and 11.9~30.1%, respectively; the consumption

is proportional to the recovery due to the coexistence of acceleration and deceleration. Electricity charging rises slightly about 14.3~30.5% with the MPR. Then, average travel time under scenarios II~VI decreases by approximately 2.6 s when compared to scenario I. It is the benefit of the T-eco-driving mode in terms of traffic efficiency.

4.2.2. Adaptability Analysis of Different Charging Lengths. Similarly, four numerical examples are used to analyze the model adaptability of different charging lengths, as shown in Table 8. When MPR is set to 40% as the constant value, charging length is set to the variable value.

The spatial-temporal trajectories under four conditions are shown in Figure 6. With the increase of WCL in the C-eco-driving mode, the vehicle's trajectory becomes completely smooth, and the fluctuation gradually decreases. The shorter charging area could cause the vehicle to drive slowly in a short period. In other words, a larger charging area can provide more charging benefits as well as a more pleasant driving experience. The trajectory in the T-eco-driving mode has not changed significantly with the WCL.

Figure 7 illustrates the electricity consumption and average travel time for two eco-driving modes under four different conditions (VII~X). For the C-eco-driving mode, the electricity consumption drops steadily with the extension of the charging lane, and the reason is that the longer the WCL, the less fluctuation in speed, as illustrated in Figure 6. The recovery of electricity is also slightly reduced due to the coexistence of acceleration and deceleration. Additionally, charging capacity increases dramatically from 1.25 kWh to 2.56 kWh as a result of the WCL extension. When the WCL is increased from 100 m to 400 m, the average travel time remains stable at about 42.5 s. This demonstrates that increasing the WCL can significantly improve energy efficiency while maintaining the same travel time. For the T-eco-driving mode, electricity consumption and recovery remain basically stable as the WCL changes in response to the trajectory's fluctuation. Similarly, according to the WCL, electricity charging increases by approximately 0.46~2.21 kWh, and the average travel time is nearly 38 s. Additionally, we compare the electricity charging and travel time between two eco-driving modes. On the one hand, while both have an upward trend in terms of charging, the C-eco-driving mode has a greater increase than the T-eco-driving mode. The T-eco-driving mode, on the other hand, has a shorter travel time than the C-eco-driving mode. Thus, both C-eco-driving and T-eco-driving modes successfully accomplish their respective objectives.

4.2.3. Adaptability Analysis of Different Charging Locations. To analyze the impact of different locations of the DWPT facilities on traffic benefits, four charging lengths (100, 200, 300, and 400 m) are used to validate the adaptability of the proposed model. This study moves the same charging length by a distance of 100 m, which simulates 15 numerical examples.

Traffic benefits of different charging locations in mixed traffic are shown in Figure 8. Firstly, for the average travel time of vehicles, when the charging area is (100, 200), the average travel time is 43.03 s. When the charging area is (400, 500), the average travel time is about 42.01 s. It can be seen that when the length has the same value, the closer the charging area is to the intersection, the shorter the average travel time. Secondly, for total electricity consumption, only when the charging area is (0, 100) and (400, 500), the electricity consumption is the positive value, and EVs passing through signalized intersections do consume additional battery electricity. Finally, the results of the three-dimensional histogram show that when the lengths are the same, the closer the DWPT facilities to the intersection, the more obvious the electricity benefits of EVs. Both evaluation indicators show that the DWPT is more profitable when it is set close to the intersection.

5. Conclusion

In this paper, a multiobjective speed planning model for CAEVs with the C-eco-driving model and T-eco-driving model is proposed, which can provide a differentiated speed guidance advice for meeting the driving strategy at signalized intersections with consideration of DWPT. The IDM calibrated by the NGSIM dataset is then used to calculate the trajectory for regular EVs. Numerical examples are used to demonstrate the proposed model's effectiveness and robustness at various scenarios of signalized intersections. For single vehicle, the T-eco-driving mode produces less speed fluctuation and travel time than the C-eco-driving mode. The C-eco-driving mode produces a more competitive charging benefit than the T-eco-driving mode. We note that adjusting the wireless charging length does not influence the results of the T-eco-driving mode. For mixed traffic, the C-eco-driving mode significantly outperforms the no guidance model in terms of charging benefit. The T-eco-driving mode significantly outperforms the no guidance model in terms of electricity consumption and average travel time. It is worth noting that the benefits of the moderate MPR have certain fluctuations and are influenced by the type of the leading vehicle. The simulation results indicate that the proposed model has a significant improvement of traffic benefits. When charging length has the same value, the closer the DWPT facilities to the intersection, the more obvious the charging benefits. Additionally, the coexistence of two eco-driving modes and human driving will result in a mutual game effect in mixed traffic, which requires extensive discussion and is the direction of future research. How to improve the cost competitive of DWPT and encourage the government as well as private enterprises to construct more DWPT facilities is also a challenge for future work.

Data Availability

The Lankershim dataset, provided by the Federal Highway Administration's NGSIM program, is used to calibrate the IDM model at signalized intersections in this study. The dataset includes detailed vehicle and road information for micro traffic flow research (http://ops.fhwa.dot.gov/traffiffifficanalysistools/ngsim.htm 2006).

Conflicts of Interest

The authors declare that they have no conflicts of interest.

Acknowledgments

This research is supported by the National Natural Science Foundation of China (No. 61703053), the National Key Research and Development Program of China (2021YFB2501200), Shaanxi Provincial Key R&D Program (2022GY-300), and the Joint Laboratory for Internet of Vehicles and Ministry of Education-China Mobile Communications Corporation.

References

[1] J. Coria, J. Bonilla, M. Grundström, and H. Pleijel, "Air pollution dynamics and the need for temporally differentiated road pricing," *Transportation Research Part A: Policy and Practice*, vol. 75, pp. 178–195, 2015.

[2] G. J. Offer, D. Howey, M. Contestabile, R. Clague, and N. P. Brandon, "Comparative analysis of battery electric, hydrogen fuel cell and hybrid vehicles in a future sustainable road transport system," *Energy Policy*, vol. 38, no. 1, pp. 24–29, 2010.

[3] J. Du and D. Ouyang, "Progress of Chinese electric vehicles industrialization in 2015: a review," *Applied Energy*, vol. 188, pp. 529–546, 2017.

[4] X. Qi, M. J. Barth, G. Wu, K. Boriboonsomsin, and P. Wang, "Energy impact of connected eco-driving on electric vehicles," in *In Road Vehicle Automation 4*, pp. 97–111, Springer, Cham, 2018.

[5] F. Song, "The impact of China's electric vehicle subsidy policy on the new energy automobile industry——based on the research on the 5 pilot cities. Wireless charging of electric vehicles in electricity and transportation networks," *IEEE Transactions on Smart Grid*, vol. 9, pp. 4503–4512, 2016.

[6] S. Lukic and Z. Pantic, "Cutting the cord: static and dynamic inductive wireless charging of electric vehicles," *IEEE Electrification Magazine*, vol. 1, no. 1, pp. 57–64, 2013.

[7] R. Tavakoli and Z. Pantic, "Analysis, design, and demonstration of a 25-kW dynamic wireless charging system for roadway electric vehicles," *IEEE Journal of Emerging and Selected Topics in Power Electronics*, vol. 6, no. 3, pp. 1378–1393, 2018.

[8] H. Zhang, Z. Hu, Z. Xu, and Y. Song, "An integrated planning framework for different types of PEV charging facilities in urban area," *IEEE Transactions on Smart Grid*, vol. 7, no. 5, pp. 2273–2284, 2016.

[9] A. Y. Lam, Y. W. Leung, and X. Chu, "Electric vehicle charging station placement: formulation, complexity, and solutions," *IEEE Transactions on Smart Grid*, vol. 5, no. 6, pp. 2846–2856, 2014.

[10] F. Ahmad, M. Saad Alam, I. Saad Alsaidan, and S. M. Shariff, "Battery swapping station for electric vehicles: opportunities and challenges," *IET Smart Grid*, vol. 3, no. 3, pp. 280–286, 2020.

[11] Z. Liu and Z. Song, "Robust planning of dynamic wireless charging infrastructure for battery electric buses," *Transportation Research Part C: Emerging Technologies*, vol. 83, pp. 77–103, 2017.

[12] A. Ahmad, M. S. Alam, and R. Chabaan, "A comprehensive review of wireless charging technologies for electric vehicles," *IEEE Transactions on Transportation Electrification*, vol. 4, no. 1, pp. 38–63, 2018.

[13] T. M. Fisher, K. B. Farley, Y. Gao, H. Bai, and Z. T. H. Tse, "Electric vehicle wireless charging technology: a state-of-the-art review of magnetic coupling systems," *Wireless Power Transfer*, vol. 1, no. 2, pp. 87–96, 2014.

[14] Z. Chen, W. Liu, and Y. Yin, "Deployment of stationary and dynamic charging infrastructure for electric vehicles along traffic corridors," *Transportation Research Part C: Emerging Technologies*, vol. 77, pp. 185–206, 2017.

[15] X. Sun, Z. Chen, and Y. Yin, "Integrated planning of static and dynamic charging infrastructure for electric vehicles," *Transportation Research Part D: Transport and Environment*, vol. 83, article 102331, 2020.

[16] S. Jeong, Y. J. Jang, and D. Kum, "Economic analysis of the dynamic charging electric vehicle," *IEEE Transactions on Power Electronics*, vol. 30, no. 11, pp. 6368–6377, 2015.

[17] Z. Chen, Y. Yin, and Z. Song, "A cost-competitiveness analysis of charging infrastructure for electric bus operations," *Transportation Research Part C: Emerging Technologies*, vol. 93, pp. 351–366, 2018.

[18] M. Fuller, "Wireless charging in California: range, recharge, and vehicle electrification," *Transportation Research Part C: Emerging Technologies*, vol. 67, pp. 343–356, 2016.

[19] Y. D. Ko and Y. J. Jang, "The optimal system design of the online electric vehicle utilizing wireless power transmission technology," *IEEE Transactions on Intelligent Transportation Systems*, vol. 14, no. 3, pp. 1255–1265, 2013.

[20] F. Musavi, M. Edington, and W. Eberle, "Wireless power transfer: a survey of EV battery charging technologies," in *2012 IEEE Energy Conversion Congress and Exposition*, pp. 1804–1810, Raleigh, NC, USA, 2012.

[21] T. Theodoropoulos, A. Amditis, J. Sallán et al., "Impact of dynamic EV wireless charging on the grid," in *2014 IEEE International Electric Vehicle Conference*, pp. 1–7, Florence, Italy, 2014.

[22] J. He, H. J. Huang, H. Yang, and T. Q. Tang, "An electric vehicle driving behavior model in the traffic system with a wireless charging lane," *Physica A: Statistical Mechanics and its Applications*, vol. 481, pp. 119–126, 2017.

[23] J. He, H. Yang, H. J. Huang, and T. Q. Tang, "Impacts of wireless charging lanes on travel time and energy consumption in a two-lane road system," *Physica A: Statistical Mechanics and its Applications*, vol. 500, pp. 1–10, 2018.

[24] J. He, H. Yang, T. Q. Tang, and H. J. Huang, "Optimal deployment of wireless charging lanes considering their adverse effect on road capacity," *Transportation Research Part C: Emerging Technologies*, vol. 111, pp. 171–184, 2020.

[25] M. Li, X. Wu, Z. Zhang, G. Yu, Y. Wang, and W. Ma, "A wireless charging facilities deployment problem considering optimal traffic delay and energy consumption on signalized arterial," *IEEE Transactions on Intelligent Transportation Systems*, vol. 20, no. 12, pp. 4427–4438, 2019.

[26] S. Mohrehkesh and T. Nadeem, "Toward a wireless charging for battery electric vehicles at traffic intersections," in *2011 14th international IEEE conference on intelligent transportation systems*, pp. 113–118, Washington, DC, USA, 2011.

[27] J. Zhang, T. Q. Tang, Y. Yan, and X. Qu, "Eco-driving control for connected and automated electric vehicles at signalized intersections with wireless charging," *Applied Energy*, vol. 282, article 116215, 2021.

[28] X. He, H. X. Liu, and X. Liu, "Optimal vehicle speed trajectory on a signalized arterial with consideration of queue,"

Transportation Research Part C: Emerging Technologies, vol. 61, pp. 106–120, 2015.

[29] F. Marini and B. Walczak, "Particle swarm optimization (PSO). A tutorial," *Chemometrics and Intelligent Laboratory Systems*, vol. 149, pp. 153–165, 2015.

[30] C. Fiori, K. Ahn, and H. A. Rakha, "Power-based electric vehicle energy consumption model: model development and validation," *Applied Energy*, vol. 168, pp. 257–268, 2016.

[31] M. Treiber, A. Hennecke, and D. Helbing, "Congested traffic states in empirical observations and microscopic simulations," *Physical Review E*, vol. 62, no. 2, pp. 1805–1824, 2000.

[32] US Federal Administration, "Next Generation Simulation Program," 2006, http://ops.fhwa.dot.gov/traffiffifficanalysistools/ngsim.htm.

[33] S. Katoch, S. S. Chauhan, and V. Kumar, "A review on genetic algorithm: past, present, and future," *Multimedia Tools and Applications*, vol. 80, no. 5, pp. 8091–8126, 2021.

[34] M. Zhu, X. Wang, A. Tarko, and S. Fang, "Modeling car-following behavior on urban expressways in Shanghai: a naturalistic driving study," *Transportation Research Part C: Emerging Technologies*, vol. 93, pp. 425–445, 2018.